

# Design and Analysis of a New Index-Modulation-aided DCSK System with Frequency-and-Time Resources

Yi Fang, *Senior Member, IEEE*, Junming Zhuo, Huan Ma, Shahid Mumtaz, *Senior Member, IEEE*, and Yonghui Li, *Fellow, IEEE*

**Abstract**—We propose a new index-modulation-aided differential chaos shift keying (DCSK) system using frequency-and-time resources, referred to as CTIM-DCSK system, to achieve high-data-rate transmissions. In the proposed system, the orthogonal sinusoidal carriers are used to transmit both the reference-chaotic and the information-bearing signals. Moreover, the frequency-and-time resources are considered as indices to carry additional information bits. To simultaneously boost the bit error rate (BER) performance and reduce the system complexity, this paper proposes a new CTIM-DCSK signal based on the frequency-and-time resources, in which the time slots used by the selected subcarriers convey the same index bits. We employ a noise-reduction method at the receiver to further improve the BER performance of the proposed CTIM-DCSK system. We also derive the theoretical BER expressions of the CTIM-DCSK system over two different channels, i.e., additive white Gaussian noise (AWGN) channel and multipath Rayleigh fading channel. We analyze the data rate, complexity and spectral efficiency of the CTIM-DCSK system in comparison with the state-of-the-art counterparts. Analytical and simulation results verify the accuracy of the theoretical analysis and the advantage of the proposed CTIM-DCSK system. Consequently, the proposed CTIM-DCSK system appears to be a competitive candidate for low-complexity Internet-of-Things applications.

**Index Terms**—Frequency-and-time index, differential chaos shift keying (DCSK), multipath Rayleigh fading channel, noise reduction.

## I. INTRODUCTION

Chaotic signal has been widely used in spread-spectrum communication systems, because of its easy generation and excellent auto-correlation properties [1], [2]. In the past few decades, chaotic communication has gained widespread attention from academia and industry. It has been proven to be one of the best candidates for wireless communications, e.g.,

Copyright (c) 2015 IEEE. Personal use of this material is permitted. However, permission to use this material for any other purposes must be obtained from the IEEE by sending a request to pubs-permissions@ieee.org.

This work was supported in part by the NSF of China under Grant 62071131, the Guangdong Basic and Applied Basic Research Foundation under Grant 2022B1515020086, the International Collaborative Research Program of Guangdong Science and Technology Department under Grant 2022A050500070, and the Industrial Research and Development Project of Haoyang Electronic Company Ltd., under Grant 2022440002001494. (Corresponding author: Yi Fang.)

Y. Fang, J. Zhuo, and H. Ma are with the School of Information Engineering, Guangdong University of Technology, China (email: fangyi@gdut.edu.cn; junmingzhuo2022@163.com; mh-zs@163.com).

S. Mumtaz is with the Instituto de Telecomunicações, 1049-001 Aveiro, Portugal, and also with Nottingham Trent University, Nottingham NG1 4BU, U.K. (e-mail: smumtaz@av.it.pt).

Y. Li is with the School of Electrical and Information Engineering, The University of Sydney, Sydney, NSW 2006, Australia (e-mail: yonghui.li@sydney.edu.au).

wireless sensor networks and wireless personal area networks due to strong anti-fading capability and low-power feature [3].

According to the requirement of chaos synchronization, the chaotic modulation schemes can be divided into two categories: coherent modulation scheme and non-coherent modulation scheme. In [4], [5], the authors have proved that two chaotic systems can be synchronized with the same parameter setting. This result has inspired more theoretical and application research of chaotic signals in communication field. As one of the coherent chaotic modulation schemes, chaos shift keying (CSK) system has been designed in [6], where a coherent receiver is employed. However, perfect chaos synchronization is still difficult to achieve in the CSK system. Therefore, most of the subsequent studies have focused on how to design chaotic communication system without requiring chaos synchronization. As a typical paradigm, a non-coherent chaotic communication system, referred to as differential CSK (DCSK) system, has been devised in [7]. Since then, it has gained a significant amount of attention in various scenarios, such as multiple input multiple output system [8], underwater acoustic communication [9], continuous mobility communication system [3], ultra-wideband (UWB) scenario [10], [11], relay-selection strategies [12], simultaneous wireless information and power transfer system [13], and bit-interleaved coded modulation system [14], [15].

The conventional DCSK system suffers from two main disadvantages. First, half of the symbol duration and energy are used to transmit reference-chaotic signal, which leads to relatively low data rate and energy efficiency. Second, the transceiver requires radio-frequency (RF) delay lines, which is hard to achieve with the existing CMOS technology. With an aim to increase the energy efficiency, the high-efficiency DCSK (HE-DCSK) system has been designed in [16]. On the other hand, a code-shifted DCSK (CS-DCSK) system has been proposed in [17], which can remove the RF delay lines. In [18], a generalized CS-DCSK (GCS-DCSK) system has been proposed to further optimize the performance of above system. An improved DCSK (I-DCSK) system has been presented in [19] to reduce the transmission duration per bit, and thus increases the data rate. By combining the transmitted-reference technique with  $M$ -ary orthogonal modulation, an orthogonal multi-level DCSK (OM-DCSK) modulation system has been devised in [20]. Thanks to this design, the OM-DCSK system can achieve higher spectral efficiency than the conventional DCSK system. For the sake of boosting the transmission throughput, an  $M$ -ary DCSK ( $M$ -DCSK) system and an  $M$ -ary code shifted DCSK (CS-MDCSK) system

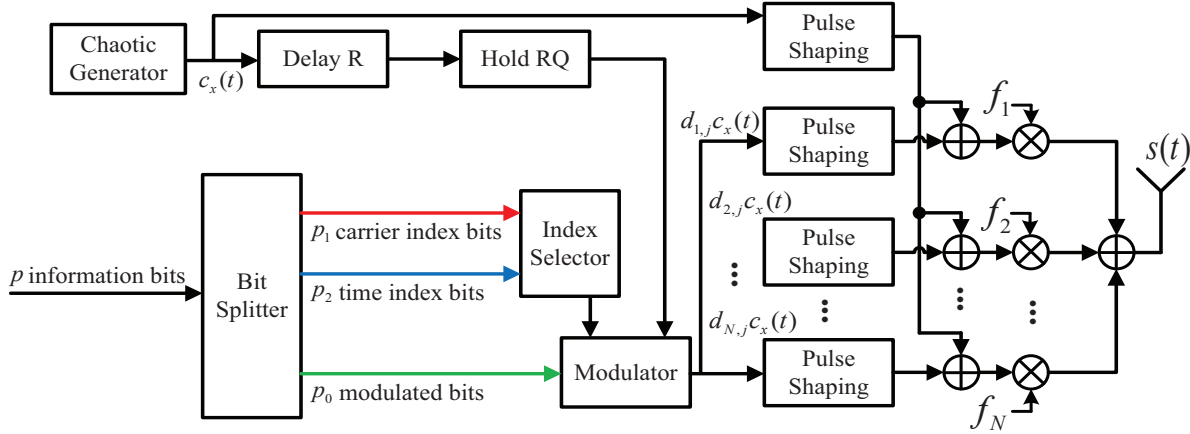


Fig. 1. Transmitter structure of the proposed CTIM-DCSK system.

have been conceived in [21] and [22], respectively. Besides, a trinal-code shifted DCSK (TCS-DCSK) system has been proposed in [23]. In this scheme, the information bits are transmitted through the Walsh code index modulation, without requiring reference-chaotic signals as the conventional DCSK system, and hence achieves higher energy efficiency. More recently, a multi-carrier DCSK (MC-DCSK) system has been proposed to achieve high-data-rate transmission [24]. This system is a parallel extension of DCSK modulation because it uses multiple subcarriers to transmit the overall signals. This structure avoids the use of a RF delay circuit at the receiver.

As another prospective modulation technique, index modulation (IM) technology has been investigated in [25]–[28], which exploits extra transmission resources to improve the spectrum efficiency, data rate, and energy efficiency. To be specific, this technology employs different system parameters to carry extra information bits. In other words, IM scheme can carry extra information bits by shifting the on-off status of different transmission entities, such as subcarriers, time slots, transmit antennas, RF mirrors, Walsh codes. For example, a spatial modulation (SM), which can carry extra information bits through the activation pattern of transmit antennas, has been proposed in [29]. In [30], a frequency index modulation (FIM) has been designed, it uses frequency instead of transmit antenna to realize the index modulation and hence enables hardware-friendly implementation. Based on the above research advancements, the IM technology has received extensive attention in 5G wireless communication [31], visible light communication (VLC) [32], orthogonal frequency-division multiplexing (OFDM) system [33], molecular communication [34], optical wireless communication [35], covert communication [36], and Internet of things (IoT) [37].

In fact, incorporating IM into DCSK modulation [38]–[41] can further enhance the system performance. For instance, combining code index modulation (CIM) and short-reference DCSK (SR-DCSK) modulation, a CIM-DCSK system has been designed in [42]. This system transmits additional information bits through the CIM. Moreover, a new GCS-DCSK system with CIM, called CIM-CS-DCSK, has been proposed in [43], which accomplishes a higher data rate than the GCS-DCSK scheme. More recently, the IM technology has also been combined with the  $M$ -ary DCSK system in [44] to realize

both high data rate and spectral efficiency. In [45], a carrier index modulation with DCSK system (CI-DCSK) has been designed. Nevertheless, in the CI-DCSK system, the number of the index carriers can only be an integer power of 2, while the number of active carriers is 1 or  $n - 1$  (i.e.,  $n + 1$  is the number of subcarriers). To resolve this problem, a generalized CI-DCSK system (GCI-DCSK) has been developed in [46]. In [47], a dual-index-modulation-aided DCSK system (DCSK-DIM) has been conceived. The DCSK-DIM system can reuse all active time slots to transmit other information bits, thus improving the data rate of the proposed system.

In addition, a new type of IM, namely multidimensional index modulation (MIM) [48], [49], has gained widespread attention recently because it can achieve high-data-rate transmissions by exploiting multiple index resources. In particular, a compressed sensing-aided multi-dimensional index modulation (i.e., CS-MIM) system has been proposed in [50]. The CS-MIM scheme uses the transmit antenna and frequency resources as the index entities to carry extra information bits, and hence improves the system capacity. In [51], a multidimensional index-aided load modulated multi-antenna (TI-MBM-LM) system has been designed. In the TI-MBM-LM system, time slots and RF mirrors are indexed simultaneously to achieve promising performance gains in load modulated multi-antenna system. Owing to the appealing advantages, the MIM technology has become an outstanding method to improve the performance of DCSK schemes. For instance, a joint time-frequency index modulation aided multiple-mode DCSK (JTIFIM-MM-DCSK) system has been proposed in [52], which can realize high-data-rate communications. In [53], a hybrid-index-modulation-aided MC-DCSK (HIM-MC-DCSK) system has been designed. It incorporates the carrier-number index modulation and carrier-index modulation into the MC-DCSK system, which can enhance the energy efficiency and spectral efficiency. More recently, a new DCSK with multidimensional index modulation (MIM-DCSK) has been proposed in [54], which exploits three dimensions of the transmission entities to convey additional information bits. Although there have been some works on MIM-aided DCSK schemes, the complexities of these systems are relatively high. Therefore, how to design a low-complexity and high-performance signal format for the MIM-aided DCSK schemes is a still challenging issue.

With this motivation, we put forward a carrier-time index-modulation-aided DCSK (CTIM-DCSK) system. Different from the previous works [52]–[54], the proposed CTIM-DCSK system proposes a new CTIM scheme to achieve lower complexity and higher transmission reliability. In particular, the proposed CTIM-DCSK system uses both the frequency and time resources as the index entities, while the HIM-MC-DCSK system [53] only uses the frequency resource as the index entity. Moreover, the proposed CTIM-DCSK system does not require the Hilbert filter exploited in [52], [53] and the Walsh-code generator exploited in [54], thus reducing the implementation complexity. In the proposed CTIM-DCSK system, the orthogonal sinusoidal carriers are used to transmit both the reference-chaotic and information-bearing signals. Moreover, in the proposed system, some extra information bits can be carried by exploiting the carrier-and-time index resources. Through such a manner, the proposed CTIM-DCSK system can exhibit desirable performance in terms of data rate and bit error rate (BER), due to the employment of two new domains of transmission resources. At the receiver, we adopt a noise-reduction operation to further improve the BER performance of the proposed system. In brief, the main contributions of this work are described as below:

- 1) We propose a new DCSK communication system based on the carrier-time index modulation (CTIM-DCSK), which exploits two additional dimensions of resources for information transmission. In this sense, the information bits are composed of three parts, i.e., the modulated bits, carrier index bits, and time index bits. In the proposed CTIM-DCSK system, the time slots used by the selected subcarriers convey the same index bits. Based on this new signal format, the proposed CTIM-DCSK system enjoys the benefits of lower complexity and higher transmission reliability with respect to the existing MIM-aided DCSK systems.
- 2) We also derive theoretical BER expressions of the CTIM-DCSK system over AWGN and multipath Rayleigh fading channels. Both theoretical and simulated results illustrate that the proposed CTIM-DCSK scheme significantly improves the BER performance with respect to the existing JTFIM-MM-DCSK, MIM-DCSK, HIM-MC-DCSK, CI-DCSK, MC-DCSK, DCSK-DIM, and conventional DCSK systems.
- 3) We analyze the data rate, complexity and spectral efficiency of the proposed CTIM-DCSK system with respect to the JTFIM-MM-DCSK, MIM-DCSK, HIM-MC-DCSK, CI-DCSK, MC-DCSK, DCSK-DIM, and conventional DCSK systems to further illustrate the superiority of our design.

The rest of this paper is structured as follows. We present the system model of the proposed CTIM-DCSK scheme in Section II. We carry out the derivation of the theoretical BER expression for the proposed system in Section III. Subsequently, the data rate, system complexity and spectral efficiency are analyzed in Section IV. The simulation results and discussions are drawn in Section V. Finally, Section VI gives a summary of this paper.

## II. SYSTEM MODEL OF PROPOSED CTIM-DCSK

### A. Transmitter

The block diagram of the transmitter for the proposed CTIM-DCSK system is given in Fig. 1. In the proposed system, we generate a length- $R$  reference-chaotic signal  $c_x = [c_{x,1}, c_{x,2}, \dots, c_{x,R}]$  by using a second-order Chebyshev polynomial function (i.e.,  $c_{k+1} = 1 - 2c_k^2$ ,  $k = 1, 2, \dots$ ). The reference-chaotic signal is transmitted in each carrier. Specifically, a CTIM-DCSK symbol contains  $p = p_0 + p_1 + p_2$  transmitted bits. In each symbol duration, since  $N - 1$  out of  $N$  subcarriers are selected to carry the carrier index bits, the number of the carrier index bits is  $p_1 = \log_2 N$ . Similarly,  $Q - 1$  out of the  $Q$  time slots are selected to carry the time index bits, thus the number of the time index bits equals  $p_2 = \log_2 Q$ . In the proposed system, each subcarrier needs an extra time slot to carry the reference-chaotic signal. As a result, there are  $Q + 1$  time slots used for transmission in each symbol duration. In addition, the number of the modulated bits becomes  $p_0 = (N - 1)(Q - 1)$ . The modulated symbols are denoted as  $\mathbf{e} = [e_1, e_2, \dots, e_r, \dots, e_{p_0}]$ ,  $r = 1, 2, \dots, p_0$ . Exploiting the index selector,  $p_1$  carrier index bits are mapped to the carrier index sequence  $\mathbf{h} = [h_1, h_2, \dots, h_\nu, \dots, h_N]$ , where  $h_\nu = 1$  represents that the  $\nu$ -th subcarrier is selected, and  $h_\nu = 0$  represents that the  $\nu$ -th subcarrier is unselected. Furthermore, the time index sequence can be represented as  $\mathbf{b} = [b_1, b_2, \dots, b_\alpha, \dots, b_Q]$ , where  $b_\alpha = 1$  or  $b_\alpha = 0$  implies that the  $\alpha$ -th time slot is selected or unselected, respectively. Specifically, suppose that  $c_l$  and  $s_l$  are two position index modulation symbols determined by the carrier index bits and time index bits, respectively. Then, the resultant carrier index sequence and time index sequence are yielded as  $[h_1, h_2, \dots, h_N] = [1, 1, \dots, 0_{c_l}, \dots, 1]$  and  $[b_1, b_2, \dots, b_Q] = [1, 1, \dots, 0_{s_l}, \dots, 1]$ , respectively.

In the modulator, every  $p$  transmitted bits are transformed to an  $N \times Q$  information matrix  $\mathbf{d} = \{d_{i,j}\}$ , where  $1 \leq i \leq N$  and  $1 \leq j \leq Q$ . If  $i \neq c_l$  and  $j \neq s_l$ ,  $d_{i,j}$  is determined by the modulated bits (i.e.,  $d_{i,j} \in \{+1, -1\}$ ); otherwise,  $d_{i,j}$  is determined by carrier index bits and time index bits (i.e.,  $d_{i,j} = 0$ ). Then,  $d_{i,j}$  is multiplied with the reference-chaotic signal  $c_x(t)$  so as to carry the information bits. Therefore, the spreading factor of the CTIM-DCSK system equals  $\beta = QR$ , where  $R$  is the length of a reference-chaotic signal. An instance of the CTIM-DCSK system with carrier and time index bits being ‘10’ and ‘11’ is given in Fig. 2. In such a scenario, the number of available carriers (resp. time slots) is 4, where 1 subcarrier (resp. time slot) is unselected. As a result, the 9 modulated bits and 4 index bits are input to modulator. In particular, the 9 modulated bits are spread by the reference-chaotic signal in the three time slots (including  $t_1, t_2, t_3$ ), and transmitted by the 3 selected subcarriers (including  $f_1, f_2$  and  $f_4$ ). On the other hand, the 4 index bits are carried by the positions (i.e., indices) of unselected carrier and unselected time slot.

Finally, both of the information-bearing signals and reference-chaotic signal  $c_x(t)$  are conveyed through the subcarrier with frequency  $f_i$ . Hence, the  $o$ -th frame of transmitted signal is written as (1), as shown at the top of the next page,

$$s(t) = \begin{cases} \sum_{i=1}^N c_x(t) \cos(2\pi f_i t + \phi_i), & (o-1)(Q+1)RT_c < t \leq ((o-1)(Q+1)+1)RT_c \\ \sum_{i=1}^N \sum_{j=1}^Q (c_x(t)d_{i,j} \cos(2\pi f_i t + \phi_i)), & ((o-1)(Q+1)+1)RT_c < t \leq ((o-1)(Q+1)+j+1)RT_c \end{cases}, \quad (1)$$

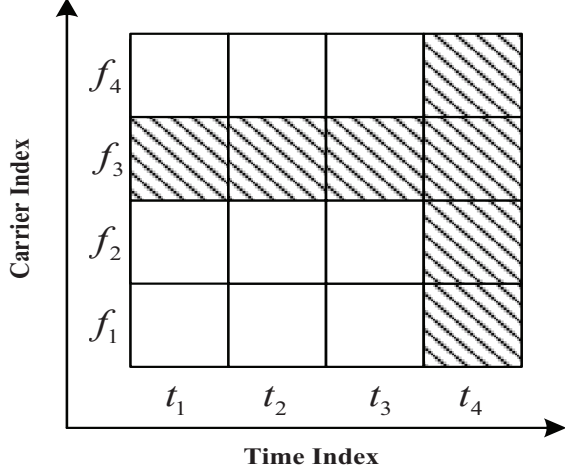


Fig. 2. An example of the CTIM-DCSK system with the carrier and time index bits are ‘10’ and ‘11’, respectively. The number of available carriers (resp. time slots) is equal to 4, where the white and shadowed boxes represent the selected and unselected subcarriers (resp. time slots), respectively.

where  $f_i$ ,  $\phi_i$  and  $T_c$  represent the frequency, the phase angle of the  $i$ -th carrier and the chip time, respectively.

### B. Receiver

In Fig. 3, the receiver of the proposed CTIM-DCSK system is illustrated. We consider a channel model of multipath Rayleigh fading channel  $\eta(t) = \sum_{l=1}^L \lambda_l \delta(t - \tau_l)$ , where  $\tau_l$  and  $\lambda_l$  are denoted as the path delay of the  $l$ -th path and the channel coefficient, respectively.  $L$  is denoted as the number of paths. The received signal output from the channel can be given as

$$r(t) = s(t) * \eta(t) + n(t), \quad (2)$$

where  $*$  is the convolution operator, and  $n(t)$  is the AWGN with zero mean and variance  $N_0/2$ . In this paper,  $\lambda_l$  is independent Rayleigh-distributed random variable. In addition, the received signals can be separated by the corresponding orthogonal carrier frequencies, and then are filtered by a set of matched filters. The demodulated discrete outputs have two parts, one part is the information bearing signals, and the other is the reference-chaotic signals. Especially, the  $N$  reference-chaotic signals are represented by a matrix  $\mathbf{A}$  with dimension of  $N \times R$ , while the  $N$  information bearing signals are represented by another matrix  $\mathbf{B}$  with dimension of  $N \times (Q \times R)$ . In order to obtain better BER performance, we can alleviate the impact of the Gaussian noise of the reference-chaotic signals by some operations. From Fig. 3, the specific operation of the noise reduction receiver is explained as below. The received reference-chaotic signals are summed and averaged. Then, the average reference-chaotic signal can be used to demodulate

the information-bearing signals. So that the average reference-chaotic signal is expressed as

$$\tilde{c}_{x,\text{ave}} = \frac{1}{N} \sum_{i=1}^N \sum_{k=1}^R \left( \sum_{l=1}^L \lambda_l c_{x,k-\tau_l} + n_{x,k}^i \right). \quad (3)$$

To facilitate the calculation, we expand the length- $R$  average reference signal  $\tilde{c}_{x,\text{ave}}$  into an  $N \times (Q \times R)$  average reference-chaotic-signal matrix  $\mathbf{X}$ . Specifically, the average reference-chaotic-signal matrix  $\mathbf{X}$  can be calculated as  $\mathbf{X} = \mathbf{I}_{N \times Q} \otimes \tilde{c}_{x,\text{ave}}$ , where  $\mathbf{I}$  is an  $N \times Q$  identity matrix. Finally, the information-bearing-signal matrix  $\mathbf{Z} = \mathbf{X} \odot \mathbf{B}$  with dimension of  $N \times (Q \times R)$  is input to the detector, where  $\odot$  is the Hadamard product [38]. The matrix  $\mathbf{Z}$  is passed through an energy detector to demodulate the modulated bits, carrier index bits and time index bits. In this detector, each row of the matrix  $\mathbf{Z}$  is divided into  $Q$  parts according to the length  $R$  of the each reference-chaotic signal. Then, the  $R$  elements of the  $j$ -th part within the  $i$ -th row of the matrix  $\mathbf{Z}$  are added up and stored in the matrix  $\mathbf{W} = \{W_{i,j}\} = [\mathbf{W}_1, \dots, \mathbf{W}_N]^T$ , where  $W_{i,j}$  ( $1 \leq i \leq N, 1 \leq j \leq Q$ ) denotes the  $j$ -th sample in the  $i$ -th subcarrier, and the superscribe ‘‘T’’ denotes the transpose operation. More specifically, the value of the  $W_{c_l,j}$  (i.e.,  $i = c_l, 1 \leq j \leq Q$ ) is calculated as

$$W_{c_l,j} \approx \sum_{k=1}^R n_{c_l,j+k} \left( \sum_{l=1}^L \lambda_l \tilde{c}_{x,\text{ave}} + n'_{i,k} \right). \quad (4)$$

Similarly, when  $j = s_l$ , and  $1 \leq i \leq N$ , the value of  $W_{i,s_l}$  can be calculated as

$$W_{i,s_l} \approx \sum_{k=1}^R n_{i,s_l+k} \left( \sum_{l=1}^L \lambda_l \tilde{c}_{x,\text{ave}} + n'_{i,k} \right). \quad (5)$$

If  $i \neq c_l$  and  $j \neq s_l$ , the element of matrix  $\mathbf{W}$  becomes

$$W_{i,j} \approx \sum_{k=1}^R \left( \sum_{l=1}^L \lambda_l \tilde{c}_{x,\text{ave}} d_{i,j} + n_{i,j+k} \right) \left( \sum_{l=1}^L \lambda_l \tilde{c}_{x,\text{ave}} + n'_{i,k} \right), \quad (6)$$

where  $n_{c_l,j+k}$ ,  $n_{i,s_l+k}$ ,  $n_{i,j+k}$ ,  $n'_{i,k}$  are independent Gaussian noises with zero mean and variance  $N_0/2$ .

1) *Carrier-Index-Bit Detection*: For recovering the carrier index bits, we need to calculate the absolute values of  $Q$  elements in the  $i$ -th row of the matrix  $\mathbf{W}$ , then sum these absolute values to obtain the decision metric for the  $i$ -th subcarrier. Thus, when  $i = c_l$ , the decision metric of the  $i$ -th subcarrier (i.e., the unselected subcarrier) can be derived as

$$V_i \approx \sum_{j=1}^Q |W_{c_l,j}|, \quad (7)$$

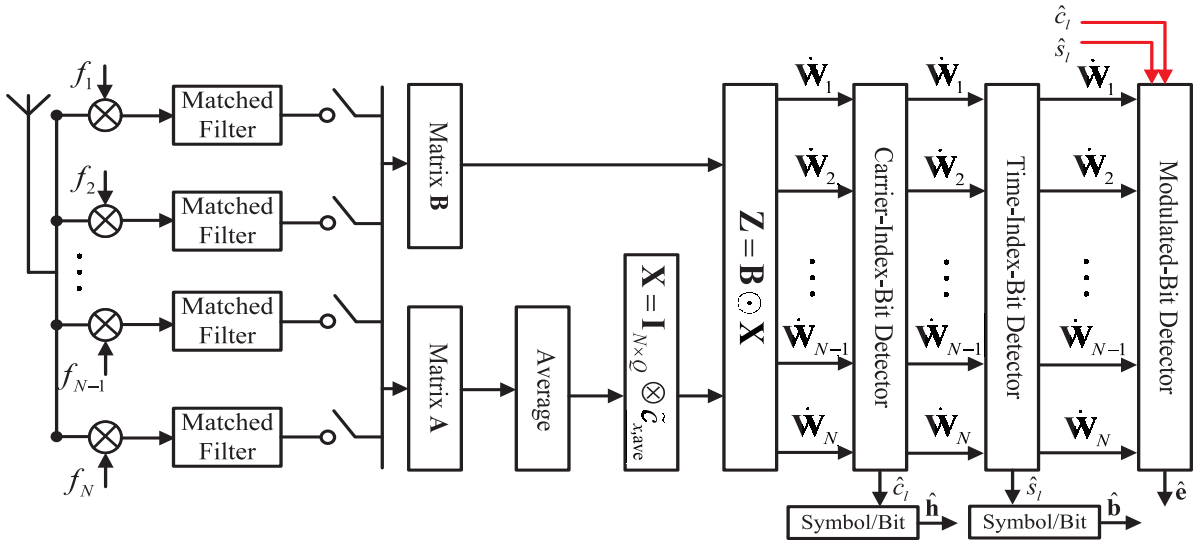


Fig. 3. Receiver structure of the proposed CTIM-DCSK system.

otherwise (when  $i \neq c_l$ ), the decision metric of the  $i$ -th subcarrier (i.e., the selected subcarrier) is expressed as

$$V'_i \approx \sum_{j=1, j \neq s_l}^Q |W_{i,j}| + |W_{i,s_l}|. \quad (8)$$

The carrier index symbol  $c_l$  can be recovered by using the position of the minimum value between the decision metrics  $V_i$  and  $V'_i$ . Mathematically, the demodulation process for the carrier index symbol can be expressed as

$$\hat{c}_l = \arg \min(V_i, V'_i), i = 1, \dots, N. \quad (9)$$

Hence, the carrier index bits are obtained by converting  $\hat{c}_l - 1$  from decimal to binary.

2) *Time-Index-Bit Detection*: To recover the time index bits, we can calculate the absolute values of  $N$  elements in the  $j$ -th column of the matrix  $\mathbf{W}$ , then sum these absolute values to obtain the decision metric for the  $j$ -th time slot. Thus, when  $j = s_l$ , the decision metric of the  $j$ -th time slot (i.e., the unselected time slot) can be expressed as

$$V_j \approx \sum_{i=1}^N |W_{i,s_l}|, \quad (10)$$

otherwise (when  $j \neq s_l$ ), the decision metric of the  $j$ -th time slot (i.e., the selected time slot) becomes

$$V'_j \approx \sum_{i=1, i \neq c_l}^N |W_{i,j}| + |W_{c_l,j}|. \quad (11)$$

Based on the position of the minimum value between the decision metrics  $V_j$  and  $V'_j$ , we can recover the time index symbol  $s_l$ . The demodulation process for the time index symbol can be given by

$$\hat{s}_l = \arg \min(V_j, V'_j), j = 1, \dots, Q. \quad (12)$$

The time index bits are obtained by converting  $\hat{s}_l - 1$  from decimal to binary.

3) *Modulated-Bit Detection*: Since the indices of carriers and time slots are detected by the aforementioned carrier-index-bit detection and time-index-bit detection, the modulated bits  $e_r$  can be estimated as

$$\hat{e}_r = \begin{cases} 1 & \text{sign}(W_{i,j}) > 0 \\ 0 & \text{otherwise} \end{cases}, \quad (13)$$

where  $r = 1, \dots, p_0$ ,  $i \neq \hat{c}_l$ , and  $j \neq \hat{s}_l$ .

### III. ANALYSIS OF BER PERFORMANCE

#### A. Formulation of System BER

In general, the overall BER of system  $P_{\text{sys}}$  is a function of the BER of carrier index bits  $P_{\text{ci}}$ , the BER of time index bits  $P_{\text{ti}}$ , and the BER of modulated bits  $P_{\text{m}}$ . To be specific, the overall BER  $P_{\text{sys}}$  can be written as

$$P_{\text{sys}} = \frac{p_1}{p} P_{\text{ci}} + \frac{p_2}{p} P_{\text{ti}} + \frac{p_0}{p} P_{\text{m}}, \quad (14)$$

where  $p = p_1 + p_2 + p_0$  is the total transmitted bits. Moreover,  $P_{\text{ci}}$ ,  $P_{\text{ti}}$  and  $P_{\text{m}}$  are the BER of carrier index bits, time index bits and modulated bits, respectively. The probability of detecting each incorrect mapped position is  $\frac{1}{2^{p_1-1}}$ , while the carrier index detection is incorrect. Similarly, when the time index detection is incorrect, the probability of detecting each incorrect mapped position is  $\frac{1}{2^{p_2-1}}$ . Thus, the expectation of the number of incorrect mapped positions for carrier index and time index can be calculated as

$$D_1 = \sum_{i=1}^{p_1} i \frac{\binom{p_1}{i}}{2^{p_1-1}}, \quad (15)$$

$$D_2 = \sum_{i=1}^{p_2} i \frac{\binom{p_2}{i}}{2^{p_2-1}}, \quad (16)$$

where  $\binom{n}{m} = \frac{n!}{m!(n-m)!}$ . The BER of the carrier index bits and time index bits can be formulated as

$$P_{\text{ci}} = \frac{D_1}{p_1} P_{\text{cd}}, \quad (17)$$

$$P_{ti} = \frac{D_2}{p_2} P_{td}. \quad (18)$$

where  $P_{cd}$  and  $P_{td}$  denote the erroneous detection probability of carrier-index and time-index modulation, respectively.

### B. Derivation of $P_{cd}$ and $P_{td}$

Without loss of generality, the modulated bit  $e_r = +1$  is transmitted in this part. Hence, the mean and the variance of  $W_{cl,j}$ ,  $W_{i,s_l}$  and  $W_{i,j}$  can be expressed by

$$u_{W_{cl,j}} = E[W_{cl,j}] \approx 0, \quad (19)$$

$$u_{W_{i,s_l}} = E[W_{i,s_l}] \approx 0, \quad (20)$$

$$u_{W_{i,j}} = E[W_{i,j}] \approx \sum_{l=1}^L \lambda_l^2 E_c, \quad (21)$$

$$\delta_{W_{cl,j}}^2 = \text{Var}[W_{cl,j}] \approx \frac{\sum_{l=1}^L \lambda_l^2 E_c N_0}{2} + \frac{N_0^2 R}{4N}, \quad (22)$$

$$\delta_{W_{i,s_l}}^2 = \text{Var}[W_{i,s_l}] \approx \frac{\sum_{l=1}^L \lambda_l^2 E_c N_0}{2} + \frac{N_0^2 R}{4N}, \quad (23)$$

$$\delta_{W_{i,j}}^2 = \text{Var}[W_{i,j}] \approx \sum_{l=1}^L \lambda_l^2 E_c N_0 \left( \frac{1}{2} + \frac{1}{2N} \right) + \frac{N_0^2 R}{4N}, \quad (24)$$

where  $E_c = \sum_{k=1}^R c_{x,k}^2$ ,  $E[\cdot]$  is the mean operator, and  $\text{Var}[\cdot]$  is the variance operator.

In the CTIM-DCSK system,  $E_b = \frac{p_0+N}{p_0+p_1+p_2} \sum_{k=1}^R c_{x,k}^2$  is the transmitted energy per bit,  $\gamma_e = \frac{\sum_{l=1}^L \lambda_l^2 E_b}{N_0}$  is the signal-to-noise ratio (SNR),  $a_0 = p_0 + N$ , and  $a_1 = p_0 + p_1 + p_2$ . As  $|W_{cl,j}|$ ,  $|W_{i,s_l}|$  and  $|W_{i,j}|$  obey the folded Gaussian distribution [42], [55], the means of  $|W_{cl,j}|$ ,  $|W_{i,s_l}|$  and  $|W_{i,j}|$  are calculated respectively as

$$\begin{aligned} u_{|W_{cl,j}|} &= \sqrt{\frac{2\delta_{W_{cl,j}}^2}{\pi}} e^{-\frac{u_{W_{cl,j}}^2}{2\delta_{W_{cl,j}}^2}} - u_{W_{cl,j}} \text{erf}\left(\frac{-u_{W_{cl,j}}}{\sqrt{2\delta_{W_{cl,j}}^2}}\right) \\ &= \sqrt{E_b N_0} \gamma_1, \end{aligned} \quad (25)$$

$$\begin{aligned} u_{|W_{i,s_l}|} &= \sqrt{\frac{2\delta_{W_{i,s_l}}^2}{\pi}} e^{-\frac{u_{W_{i,s_l}}^2}{2\delta_{W_{i,s_l}}^2}} - u_{W_{i,s_l}} \text{erf}\left(\frac{-u_{W_{i,s_l}}}{\sqrt{2\delta_{W_{i,s_l}}^2}}\right) \\ &= \sqrt{E_b N_0} \gamma_1, \end{aligned} \quad (26)$$

$$\begin{aligned} u_{|W_{i,j}|} &= \sqrt{\frac{2\delta_{W_{i,j}}^2}{\pi}} e^{-\frac{u_{W_{i,j}}^2}{2\delta_{W_{i,j}}^2}} - u_{W_{i,j}} \text{erf}\left(\frac{-u_{W_{i,j}}}{\sqrt{2\delta_{W_{i,j}}^2}}\right) \\ &= \sqrt{E_b N_0} \gamma, \end{aligned} \quad (27)$$

where  $\text{erf}(\cdot)$  is the error function,

$$\gamma_1 = \sqrt{\frac{a_1}{\pi a_0} + \frac{R}{2\pi\gamma_e N}}, \quad (28)$$

$$\begin{aligned} \gamma &= \sqrt{\frac{a_1(N+1)}{\pi a_0 N} + \frac{R}{2\pi\gamma_e N}} e^{-\left(\frac{1}{\frac{a_0(N+1)}{\gamma_e a_1 N} + \frac{R a_0^2}{2\gamma_e^2 a_1^2 N}}\right)} \\ &\quad - \sqrt{\gamma_e} \frac{a_1}{a_0} \text{erf}\left(-\sqrt{\frac{1}{\frac{a_0(N+1)}{\gamma_e a_1 N} + \frac{R a_0^2}{2\gamma_e^2 a_1^2 N}}}\right). \end{aligned} \quad (29)$$

Furthermore, the variances of  $|W_{cl,j}|$ ,  $|W_{i,s_l}|$  and  $|W_{i,j}|$  can be calculated respectively as

$$\begin{aligned} \delta_{|W_{cl,j}|}^2 &= u_{W_{cl,j}}^2 + \delta_{W_{cl,j}}^2 - u_{|W_{cl,j}|}^2 \\ &= E_b N_0 \left( \frac{a_1}{2a_0} + \frac{R}{4\gamma_e} - \gamma_1^2 \right) = E_b N_0 \rho_1, \end{aligned} \quad (30)$$

$$\begin{aligned} \delta_{|W_{i,s_l}|}^2 &= u_{W_{i,s_l}}^2 + \delta_{W_{i,s_l}}^2 - u_{|W_{i,s_l}|}^2 \\ &= E_b N_0 \left( \frac{a_1}{2a_0} + \frac{R}{4\gamma_e} - \gamma_1^2 \right) = E_b N_0 \rho_1, \end{aligned} \quad (31)$$

$$\begin{aligned} \delta_{|W_{i,j}|}^2 &= u_{W_{i,j}}^2 + \delta_{W_{i,j}}^2 - u_{|W_{i,j}|}^2 \\ &= E_b N_0 \left( \frac{\gamma_e a_1^2}{a_0^2} + \frac{a_1}{a_0} + \frac{R}{4\gamma_e} - \gamma^2 \right) = E_b N_0 \rho, \end{aligned} \quad (32)$$

where

$$\rho_1 = \left( \frac{a_1}{2a_0} + \frac{R}{4\gamma_e N} - \gamma_1^2 \right), \quad (33)$$

$$\rho = \left( \frac{\gamma_e a_1^2}{a_0^2} + \frac{a_1(N+1)}{2a_0 N} + \frac{R}{4\gamma_e N} - \gamma^2 \right). \quad (34)$$

Thus, the means of  $V_i$  and  $V_i'$  can be written as

$$u_{V_i} = Q \cdot u_{|W_{cl,j}|} = Q \sqrt{E_b N_0} \gamma_1, \quad (35)$$

$$\begin{aligned} u_{V_i'} &= (Q-1)u_{|W_{i,j}|} + u_{|W_{i,s_l}|} \\ &= (Q-1)\sqrt{E_b N_0} \gamma + \sqrt{E_b N_0} \gamma_1. \end{aligned} \quad (36)$$

Similarly, the mean of  $V_j$  and  $V_j'$  can also be given by

$$u_{V_j} = N \cdot u_{|W_{i,s_l}|} = N \sqrt{E_b N_0} \gamma_1, \quad (37)$$

$$\begin{aligned} u_{V_j'} &= (N-1)u_{|W_{i,j}|} + u_{|W_{cl,j}|} \\ &= (N-1)\sqrt{E_b N_0} \gamma + \sqrt{E_b N_0} \gamma_1. \end{aligned} \quad (38)$$

According to (4), (5), (7), and (10), the components of the decision metrics  $V_i$  and  $V_j$  are only related to Gaussian noises, and hence are independent of one another. As such, the variances of  $V_i$  and  $V_j$  can be given by

$$\delta_{V_i}^2 = Q \cdot \delta_{|W_{cl,j}|}^2 = E_b N_0 \rho_1 Q, \quad (39)$$

$$\delta_{V_j}^2 = N \cdot \delta_{|W_{i,s_l}|}^2 = E_b N_0 \rho_1 N. \quad (40)$$

On the other hand, the components of  $V_i'$  (resp.  $V_j'$ ) are calculated using the same average reference-chaotic signal at the noise-reduction receiver. Thus, the variables  $|W_{i,1}|, \dots, |W_{i,s_l-1}|, |W_{i,s_l+1}|, \dots, |W_{i,Q}|$  (resp.  $|W_{1,j}|, \dots, |W_{c_l-1,j}|, |W_{c_l+1,j}|, \dots, |W_{N,j}|$ ) are correlated with one another. In this system,  $\delta_{|W_{i,j}|}^2$  and  $E(|W_{i,j}|)$  can be calculated, while  $E(|W_{i,j}|, |W_{i,j'}|)$  (resp.  $E(|W_{i,j}|, |W_{i',j}|)$ ) cannot be calculated by the formula derivation, where  $j \neq j'$  (resp.  $i \neq i'$ ). Hence, we resort to the Monte-Carlo simulation to obtain the corresponding expectation, which is denoted by  $\zeta$ . Based on the above analysis, the variance of  $V_i'$  and  $V_j'$  are calculated respectively as

$$\begin{aligned} \delta_{V_i'}^2 &= (Q-1)\delta_{|W_{i,j}|}^2 + \delta_{|W_{i,s_l}|}^2 + 2 \binom{Q-1}{2} (\zeta - u_{|W_{i,j}|} u_{|W_{i,j'}|}) \\ &= (Q-1) E_b N_0 \rho + E_b N_0 \rho_1 + 2 \binom{Q-1}{2} (\zeta - E_b N_0 \gamma^2), \end{aligned} \quad (41)$$

$$\begin{aligned} \delta_{V_j'}^2 &= (N-1)\delta_{|W_{i,j}|}^2 + \delta_{|W_{i,c_l}|}^2 + 2 \binom{N-1}{2} (\zeta - u_{|W_{i,j}|} u_{|W_{i',j}|}) \\ &= (N-1) E_b N_0 \rho + E_b N_0 \rho_1 + 2 \binom{N-1}{2} (\zeta - E_b N_0 \gamma^2). \end{aligned} \quad (42)$$

In the proposed CTIM-DCSK system, if the decision metric  $V_i$  is larger than the minimum of the decision metric  $V_i'$ , an error occurs. Based on the cumulative distribution function (CDF) and the probability density function (PDF) of two decision metrics, the erroneous detection probability of the carrier-index modulation can be given as [56], [57]

$$\begin{aligned} P_{cd} &= \Pr[V_i > \min(V_i')] \\ &= \int_0^{+\infty} (1 - (1 - F_{V_i'}(y))^{2^{p_1}-1}) f_{V_i}(y) dy, \end{aligned} \quad (43)$$

where  $f_{V_i}(y)$  represents the PDF of  $V_i$  and  $F_{V_i'}(y)$  represents the CDF of  $V_i'$ . The  $2^{p_1} - 1$  correlator outputs are independent of one another and have identically distributed. So that  $\min(V_i')$  is the minimum order statistic and its CDF can be given as  $(1 - (1 - F_{V_i'}(y))^{2^{p_1}-1})$ . Since the summation of several independent folded-Gaussian-distributed random variables follows a Gaussian distribution, the PDF of  $V_i$  and CDF of  $V_i'$  are calculated respectively as

$$f_{V_i}(y) = \frac{1}{\sqrt{2\pi\delta_{V_i}^2}} \exp\left(-\frac{(y - u_{V_i})^2}{2\delta_{V_i}^2}\right), \quad (44)$$

$$F_{V_i'}(y) = \frac{1}{2} \left(1 + \operatorname{erf}\left(\frac{(y - u_{V_i'})}{\sqrt{2\delta_{V_i'}^2}}\right)\right). \quad (45)$$

Based on (44) and (45), (43) is simplified as (46), as shown at the top of the following page. Let  $u = \frac{y}{\sqrt{E_b N_0}}$ ,  $\eta_1 = 2 \binom{Q-1}{2} \left(\frac{\zeta}{E_b N_0} - \gamma^2\right)$ , and  $\eta_2 = 2 \binom{N-1}{2} \left(\frac{\zeta}{E_b N_0} - \gamma^2\right)$ , the erroneous detection probability can be further reduced as (47), as shown at the top of the following page.

Similarly, the erroneous detection probability of the time-index modulation can be expressed as

$$\begin{aligned} P_{td} &= \Pr[V_j > \min(V_j')] \\ &= \int_0^{+\infty} (1 - (1 - F_{V_j'}(y))^{2^{p_2}-1}) f_{V_j}(y) dy, \end{aligned} \quad (48)$$

where the decision metrics  $V_j$  and  $V_j'$  follow Gaussian distributions. Thus, the PDF of  $V_j$  and the CDF of  $V_j'$  can be given respectively as

$$f_{V_j}(y) = \frac{1}{\sqrt{2\pi\delta_{V_j}^2}} \exp\left(-\frac{(y - u_{V_j})^2}{2\delta_{V_j}^2}\right), \quad (49)$$

$$F_{V_j'}(y) = \frac{1}{2} \left(1 + \operatorname{erf}\left(\frac{(y - u_{V_j'})}{\sqrt{2\delta_{V_j'}^2}}\right)\right). \quad (50)$$

In a word, the erroneous detection probability  $P_{td}$  is simplified as (51), as shown at the top of the following page. Let  $u = \frac{y}{\sqrt{E_b N_0}}$ ,  $\eta_1 = 2 \binom{Q-1}{2} \left(\frac{\zeta}{E_b N_0} - \gamma^2\right)$ , and  $\eta_2 = 2 \binom{N-1}{2} \left(\frac{\zeta}{E_b N_0} - \gamma^2\right)$ , (51) can be further reduced as (52), as shown at the top of the following page.

Moreover, The BER of a DCSK system  $P_e$  can be expressed

$$P_e = \frac{1}{2} \operatorname{erfc}\left(\left[\frac{(N+1)a_0}{N a_1 \gamma_e} + \frac{R a_0^2}{2\gamma_e^2 a_1^2 N}\right]^{-\frac{1}{2}}\right). \quad (53)$$

For the modulated bits, there are four different scenarios which may cause erroneous detection. In the first scenario, the modulated bits are detected incorrectly, but the index bits are demodulated correctly. In the second scenario, the carrier index bits are detected incorrectly. In the third scenario, the time index bits are detected incorrectly. In the fourth scenario, both the time index detection and the carrier index detection are detected incorrectly. Therefore, the BER for modulated bits is calculated as (54), as shown at the top of the following page.

We consider that the multipath Rayleigh fading channel is an independent and identically distributed channel. Thereby, the PDF of the instantaneous SNR  $\gamma_e$  can be expressed by

$$f(\gamma_e) = \frac{\gamma_e^{L-1}}{(L-1)! \bar{\gamma}_a^L} \exp\left(-\frac{\gamma_e}{\bar{\gamma}_a}\right), \quad (55)$$

where  $\bar{\gamma}_a = \frac{E_b}{N_0} E[\lambda_i^2] = \frac{E_b}{N_0} E[\lambda_l^2]$ ,  $i \neq l$  represents the average instantaneous SNR per channel, and  $\gamma_e = \frac{E_b}{N_0} \left(\sum_{l=1}^L \lambda_l^2\right)$  with  $\sum_{l=1}^L \lambda_l^2 = 1$ .

Hence, the average BER of the proposed CTIM-DCSK system over a multipath Rayleigh fading channel is formulated as

$$P_{\text{mul}} = \int_0^{+\infty} P_{\text{sys}} \cdot f(\gamma_e) d\gamma_e. \quad (56)$$

#### IV. ANALYSIS OF COMPLEXITY AND EFFICIENCY

The data rate, complexity and spectral efficiency of the CTIM-DCSK system are calculated, then the proposed system is compared with the JTFIM-MM-DCSK system [52], MIM-DCSK system [54], HIM-MC-DCSK system [53], CI-DCSK system [45], MC-DCSK system [24], DCSK-DIM system [47], and conventional DCSK system [7]. In the analysis, the data rate can be defined as the ratio of overall number of transmitted bits to transmission duration per symbol. According to Section II-A, the carrier and time indices are used to transmit some

$$P_{\text{cd}} = \frac{1}{\sqrt{2\pi E_b N_0 \rho_1 Q}} \int_0^{+\infty} \left[ 1 - \left( \frac{1}{2} - \frac{1}{2} \operatorname{erf} \left( \frac{(y - [(Q-1)(\sqrt{E_b N_0} \gamma) + \sqrt{E_b N_0} \gamma_1])}{\sqrt{2[(Q-1)(E_b N_0 \rho) + E_b N_0 \rho_1 + 2(Q_2^{-1})(\zeta - E_b N_0 \gamma^2)]}} \right) \right)^{2^{p_1}-1} \right] \times \exp \left( -\frac{(y - Q\sqrt{E_b N_0} \gamma_1)^2}{2\rho_1 Q} \right) dy, \quad (46)$$

$$P_{\text{cd}} = \frac{1}{\sqrt{2\pi \rho_1 Q}} \int_0^{+\infty} \left[ 1 - \left( \frac{1}{2} - \frac{1}{2} \operatorname{erf} \left( \frac{(u - [(Q-1)\gamma + \gamma_1])}{\sqrt{2[(Q-1)\rho + \rho_1 + \eta_1]}} \right) \right)^{2^{p_1}-1} \right] \times \exp \left( -\frac{(u - Q\gamma_1)^2}{2\rho_1 Q} \right) du, \quad (47)$$

$$P_{\text{td}} = \frac{1}{\sqrt{2\pi E_b N_0 \rho_1 N}} \int_0^{+\infty} \left[ 1 - \left( \frac{1}{2} - \frac{1}{2} \operatorname{erf} \left( \frac{(y - [(N-1)(\sqrt{E_b N_0} \gamma) + \sqrt{E_b N_0} \gamma_1])}{\sqrt{2[(N-1)(E_b N_0 \rho) + E_b N_0 \rho_1 + 2(N_2^{-1})(\zeta - E_b N_0 \gamma^2)]}} \right) \right)^{2^{p_2}-1} \right] \times \exp \left( -\frac{(y - N\sqrt{E_b N_0} \gamma_1)^2}{2\rho_1 N} \right) dy, \quad (51)$$

$$P_{\text{td}} = \frac{1}{\sqrt{2\pi \rho_1 N}} \int_0^{+\infty} \left[ 1 - \left( \frac{1}{2} - \frac{1}{2} \operatorname{erf} \left( \frac{(u - [(N-1)\gamma + \gamma_1])}{\sqrt{2[(N-1)\rho + \rho_1 + \eta_2]}} \right) \right)^{2^{p_2}-1} \right] \times \exp \left( -\frac{(u - N\gamma_1)^2}{2\rho_1 N} \right) du, \quad (52)$$

$$P_m = P_e(1 - P_{\text{cd}})(1 - P_{\text{td}}) + \frac{(0.5 + P_e(p_1 - 1))}{p_1} P_{\text{cd}}(1 - P_{\text{td}}) + \frac{(0.5 + P_e(p_2 - 1))}{p_2} P_{\text{td}}(1 - P_{\text{cd}}) + \frac{P_e(N-2)(Q-2) + 0.5(p_0 - (N-2)(Q-2))}{p_0} P_{\text{td}}P_{\text{cd}}. \quad (54)$$

extra information bits in the proposed CTIM-DCSK system. To be specific, the number of index bits is  $\log_2 N + \log_2 Q$ , while the number of modulated bits is  $(N-1)(Q-1)$ . Therefore, the total number of transmitted bits becomes  $\log_2 N + \log_2 Q + (N-1)(Q-1)$ . Since the transmission duration for each CTIM-DCSK system is  $R(Q+1)T_c$ , the expression of data rate is written as  $\varepsilon_1 = \frac{Q(\log_2 N + \log_2 Q + p_0)}{\beta(Q+1)T_c}$ . In addition, the data rate of the JTFIM-MM-DCSK system can be calculated as  $\varepsilon_2 = \frac{\log_2 C_N^{N_s} + N_s \log_2 C_Q^{Q_s} + (N-N_s)Q + N_s[Q_s + 2(Q-Q_s)]}{\beta T_c}$ , where  $N_s$  and  $Q_s$  are defined as the number of selected subcarriers and the number of selected time slots, respectively,  $C_m^n = \frac{n!}{m!(n-m)!}$  is the binomial coefficient. Similarly, the data rate of the MIM-DCSK system is calculated as  $\varepsilon_3 = \frac{Q[\log_2 N + (N-1)\log_2 Q + (N-1)\log_2 M + (Q-1)(N-1)]}{(Q+1)\beta T_c}$ , where  $M$  is the  $M$ -order of Walsh code. Furthermore, the data rates of the HIM-MC-DCSK, CI-DCSK, MC-DCSK, DCSK-DIM and conventional DCSK systems are summarized in the Table I.

In Fig. 4 and Fig. 5, the data rate of the proposed CTIM-DCSK system is compared with those of its competitors versus. It can be clearly observed that the CTIM-DCSK system has a higher data rate than its competitors except for the JTFIM-MM-DCSK system and the MIM-DCSK system. Although the data rate of the CTIM-DCSK system is lower than those of the JTFIM-MM-DCSK system and the MIM-DCSK

system, the complexities of latter two systems are significantly higher. To be specific, the complexities per transmitted bit for the JTFIM-MM-DCSK system and MIM-DCSK system are almost three times and twice of the proposed CTIM-DCSK system, respectively. In addition, with the similar data rate, the BER performance of the proposed CTIM-DCSK system is significantly better than those of the JTFIM-MM-DCSK system and the MIM-DCSK system (see the forthcoming Fig. 6, Fig. 13, and Fig. 14).

On the other hand, the system complexity is composed of two parts, including the complexity of spreading/despreading operations of the system and the complexity of index-search. In particular, the index-search complexity is defined as the number of comparison operations required to detect the activation patterns of transmission entities (e.g., carriers and time slots). In the proposed CTIM-DCSK system, it needs to generate  $N$  reference-chaotic signals, so that the spreading/despreading complexity is  $((N-1)(Q-1) + N)R$ . In addition, the index-search complexity of the CTIM-DCSK system is  $C_N^1 + C_Q^1$ . Therefore, the complexity of the CTIM-DCSK system becomes  $[(N-1)(Q-1) + N]R + C_N^1 + C_Q^1$ . In addition, Table I illustrates the complexities of the JTFIM-MM-DCSK system, MIM-DCSK system, HIM-MC-DCSK system, CI-DCSK system, MC-DCSK system, DCSK-DIM

TABLE I

DATA RATE AND COMPLEXITY COMPARISON AMONG THE PROPOSED CTIM-DCSK SYSTEM, JTFIM-MM-DCSK SYSTEM, MIM-DCSK SYSTEM, HIM-MC-DCSK SYSTEM, CI-DCSK SYSTEM, MC-DCSK SYSTEM, DCSK-DIM SYSTEM, AND CONVENTIONAL DCSK SYSTEM

System	Data Rate	Complexity
CTIM-DCSK	$\frac{Q[\log_2 N + \log_2 Q + (N-1)(Q-1)]}{\beta(Q+1)T_c}$	$[(N-1)(Q-1) + N]R + C_N^1 + C_Q^1$
JTFIM-MM-DCSK	$\frac{\log_2 C_N^{N_s} + N_s \log_2 C_Q^{Q_s} + (N-N_s)Q + N_s[Q_s + 2(Q-Q_s)]}{\beta T_c}$	$2\{(N-N_s)Q + N_s[Q_s + 2(Q-Q_s)] + NQ\}R$
MIM-DCSK	$\frac{Q[\log_2 N + (N-1)\log_2 Q + (N-1)\log_2 M + (Q-1)(N-1)]}{(Q+1)\beta T_c}$	$(N-1)QR + R + (N-1)MR + (N-1)(C_M^1 + C_Q^1) + C_N^1$
HIM-MC-DCSK	$\frac{2N}{\beta T_c}$	$(3+N)\beta + NC_{\frac{1}{2}}^1$
CI-DCSK	$\frac{N-1+\log_2 N}{\beta T_c}$	$NR + C_N^1$
MC-DCSK	$\frac{N}{\beta T_c}$	$(N+1)R$
DCSK-DIM	$\frac{2(Q-1+\log_2 Q)}{\beta T_c}$	$(2Q+1)R + 2C_Q^1$
DCSK	$\frac{1}{\beta T_c}$	$2R$

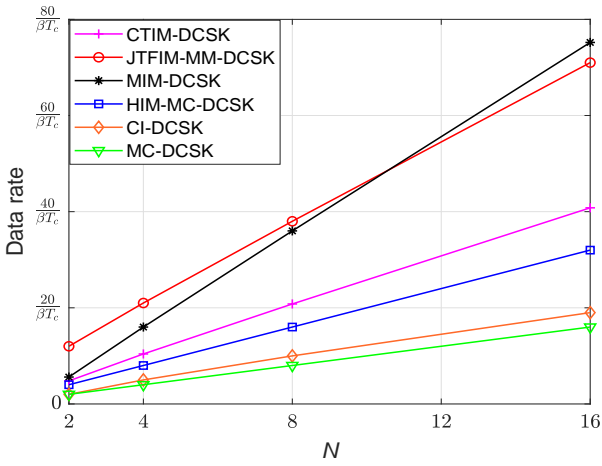


Fig. 4. Data rates of the proposed CTIM-DCSK system ( $Q = 4$ ), JTFIM-MM-DCSK system ( $N_s = 1, Q = 4, Q_s = 3$ ), MIM-DCSK system ( $Q = 4, M = 4$ ), HIM-MC-DCSK system, CI-DCSK system, and MC-DCSK system with different numbers of subcarriers  $N$ .

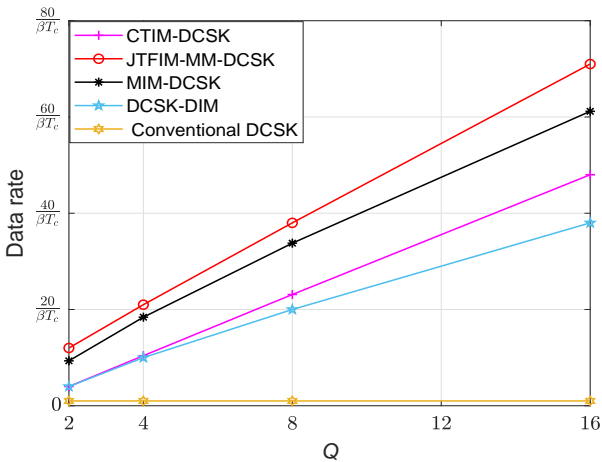


Fig. 5. Data rates of the proposed CTIM-DCSK system ( $N = 4$ ), JTFIM-MM-DCSK system ( $N = 4, N_s = 1, Q_s = Q - 1$ ), MIM-DCSK system ( $N = 4, M = 4$ ), DCSK-DIM system, and conventional DCSK system with different numbers of time slots  $Q$ .

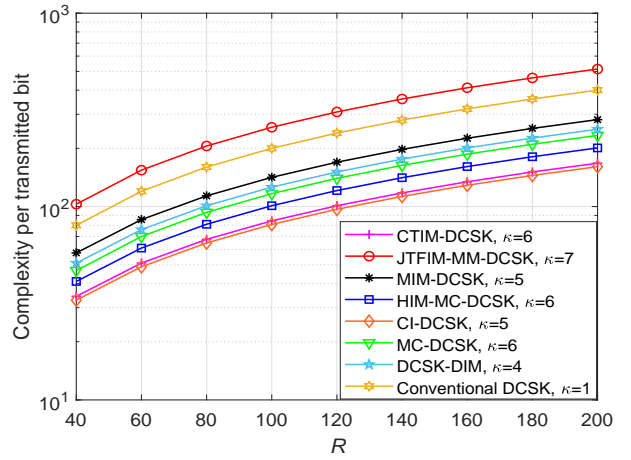


Fig. 6. Complexities per transmitted bit of the proposed CTIM-DCSK, JTFIM-MM-DCSK, MIM-DCSK, HIM-MC-DCSK, CI-DCSK, MC-DCSK, DCSK-DIM, and conventional DCSK systems versus the parameter  $R$ .

system, and conventional DCSK system. As a further investigation, the complexities per transmitted bit for different DCSK systems versus the length  $R$  of reference-chaotic signal are shown in Fig. 6, where  $\kappa$  denotes the number of transmitted bits per symbol. Here, the simulation parameters of the CTIM-DCSK system are set as  $N = 2$  and  $Q = 4$ , while those of the JTFIM-MM-DCSK, MIM-DCSK, HIM-MC-DCSK, CI-DCSK, MC-DCSK and DCSK-DIM systems are set as  $N/N_s/Q/Q_s = 2/1/2/1$ ,  $N/Q/M = 2/2/4$ ,  $N = 3$ ,  $N = 4$ ,  $N = 6$ ,  $Q = 2$ , respectively. It should be noted that  $\kappa$  cannot be set to a constant for all the considered DCSK schemes in this paper because of their inherent characteristics. As shown, the complexity of the CTIM-DCSK system is lower than those of the JTFIM-MM-DCSK, MIM-DCSK, HIM-MC-DCSK, MC-DCSK, DCSK-DIM, and conventional DCSK systems, but is slightly higher than the CI-DCSK system.

Spectral efficiency is also an important performance metric for wireless communication systems. In general, the spectral efficiency can be defined as the ratio of the data rate to overall bandwidth [38], [58]. The spectral efficiencies of the CTIM-DCSK system and its competitors are calculated and shown in Table II, where  $\omega$  is the bandwidth of the subcarrier. It is

TABLE II

SPECTRAL EFFICIENCY COMPARISON AMONG THE PROPOSED CTIM-DCSK SYSTEM, JTFIM-MM-DCSK SYSTEM, MIM-DCSK SYSTEM, HIM-MC-DCSK SYSTEM, CI-DCSK SYSTEM, MC-DCSK SYSTEM, DCSK-DIM SYSTEM, AND CONVENTIONAL DCSK SYSTEM

System	Spectral Efficiency
CTIM-DCSK	$\frac{\varepsilon_1}{N\omega}$
JTFIM-MM-DCSK	$\frac{\varepsilon_2}{(N+1)\omega}$
MIM-DCSK	$\frac{\varepsilon_3}{N\omega}$
HIM-MC-DCSK	$\frac{2N}{(N+1)\beta T_c \omega}$
CI-DCSK	$\frac{N-1+\log_2 N}{(N+1)\beta T_c \omega}$
MC-DCSK	$\frac{N}{(N+1)\beta T_c \omega}$
DCSK-DIM	$\frac{2(Q-1+\log_2 Q)}{\beta T_c \omega}$
DCSK	$\frac{1}{\beta T_c \omega}$

obvious from Fig. 7 and Fig. 8 that the spectral efficiency of the CTIM-DCSK system is higher than those of the HIM-MC-DCSK, CI-DCSK, MC-DCSK and conventional DCSK systems, but lower than those of the JTFIM-MM-DCSK, MIM-DCSK, DCSK-DIM systems. The reason is that the spectral efficiency is proportional to the data rate when using the same bandwidth. Actually, the proposed CTIM-DCSK system can get desirable benefits from BER performance and complexity at the price of sacrificing some spectral efficiency.

## V. NUMERICAL RESULTS AND DISCUSSIONS

The theoretical and simulated BER performance of the proposed system are evaluated over AGWN and multipath Rayleigh fading channels in this section. Moreover, we compare the BER performance of the proposed CTIM-DCSK system with the CI-DCSK system [45], MC-DCSK system [24], DCSK-DIM system [47], JTFIM-MM-DCSK system [52], MIM-DCSK system [54] and HIM-MC-DCSK system [53]. In all figures,  $\beta$  represents the spreading factor and  $\varepsilon$  represents the data rate. In a multipath Rayleigh fading channel, we are set: the fading path  $L = 3$ , the same average power gains  $E[\lambda_1^2] = E[\lambda_2^2] = E[\lambda_3^2] = 1/3$ , and the path delays  $\tau_1 = 0$ ,  $\tau_2 = 1$  and  $\tau_3 = 2$ . The simulation parameters of CTIM-DCSK system are set as  $N = 4$ ,  $Q = 4$  and  $N = 8$ ,  $Q = 4$  for  $\varepsilon = \frac{10}{\beta T_c}$  and  $\varepsilon = \frac{20}{\beta T_c}$ , respectively.

Fig. 9 shows the theoretical and simulated BER performance of the proposed CTIM-DCSK over AWGN and multipath Rayleigh fading channels, as well as the effect of parameters  $N$  and  $Q$  on the BER performance of the CTIM-DCSK system. As shown, the simulation results match very well with theoretical BER expressions, confirming the accuracy of our theoretical analysis. On the one hand, when the number of time slots  $Q$  and spreading factor  $\beta$  are fixed, the BER performance of the CTIM-DCSK system gets better as the number of subcarriers  $N$  increases from 4 to 8. On the other hand, when the number of subcarriers  $N$  and  $\beta$  are fixed, the BER performance of the CTIM-DCSK system improves as the number of time slots  $Q$  increases from 4 to 8. For example, in an AWGN channel, when  $N$  and  $\beta$  are fixed, the CTIM-DCSK system with  $Q = 8$  achieves a gain of 1.5 dB over that with  $Q = 4$  at a BER of  $10^{-5}$ .

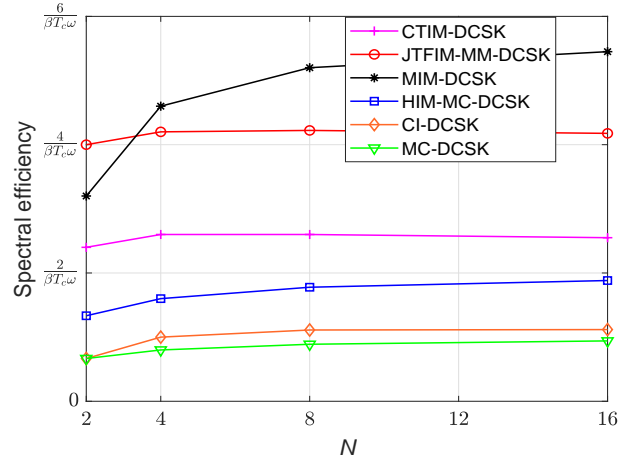


Fig. 7. Spectral efficiencies of the proposed CTIM-DCSK system ( $Q = 4$ ), JTFIM-MM-DCSK system ( $N_s = 1, Q = 4, Q_s = 3$ ), MIM-DCSK system ( $Q = 4, M = 4$ ), HIM-MC-DCSK system, CI-DCSK system, and MC-DCSK system with different numbers of subcarriers  $N$ .

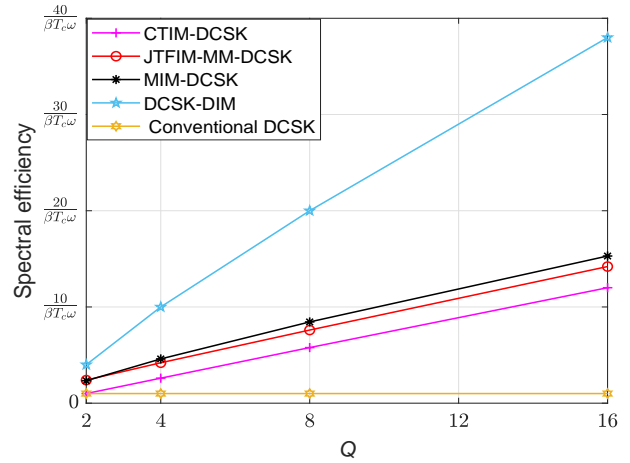


Fig. 8. Spectral efficiencies of the proposed CTIM-DCSK system ( $N = 4$ ), JTFIM-MM-DCSK system ( $N = 4, N_s = 1, Q_s = Q - 1$ ), MIM-DCSK system ( $N = 4, M = 4$ ), DCSK-DIM system, and conventional DCSK system with different numbers of time slots  $Q$ .

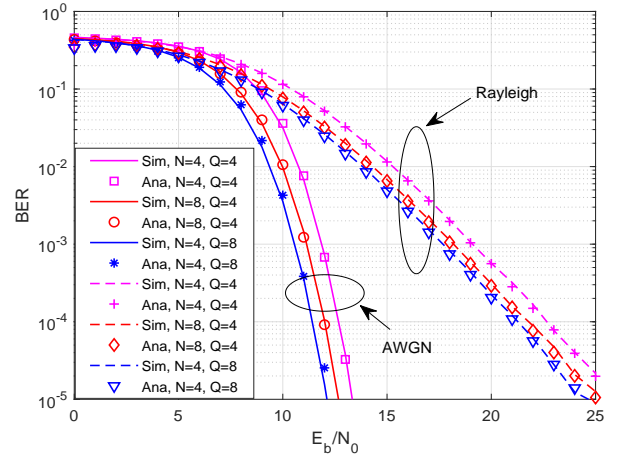


Fig. 9. Theoretical and simulation BER performance of the proposed CTIM-DCSK system over AWGN as well as multipath Rayleigh fading channels, where  $\beta = 800$ .

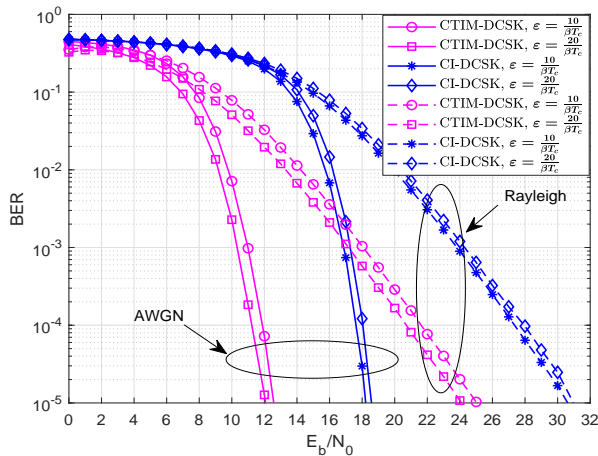


Fig. 10. BER performance of the proposed CTIM-DCSK and CI-DCSK systems over AWGN and multipath Rayleigh fading channels, where  $\beta = 450$ .

We compare the BER performance of the proposed CTIM-DCSK system and the CI-DCSK system in Fig. 10, where the data rate and spread factor are set to  $\varepsilon = \frac{10}{\beta T_c}$ ,  $\frac{20}{\beta T_c}$  and  $\beta = 450$ .<sup>1</sup> Referring to this figure, the BER performance of the CTIM-DCSK system outperforms that of the CI-DCSK system over AWGN as well as multipath Rayleigh fading channels. For instance, when  $\varepsilon = \frac{10}{\beta T_c}$ , the performance improvement for CTIM-DCSK system is about 5.5 dB with respect to CI-DCSK system over the AWGN channel at a BER of  $10^{-5}$ . Furthermore, the CTIM-DCSK system can have a gain of about 5 dB compared with the CI-DCSK system at the same BER level over the multipath Rayleigh fading channel. In addition, when  $\varepsilon$  increases from  $\frac{10}{\beta T_c}$  to  $\frac{20}{\beta T_c}$ , the performance of the CTIM-DCSK system slightly improves, while that of the CI-DCSK system slightly degrades. The reason is that the number of reference-chaotic signals (i.e., the number of carriers) increases as the data rate becomes larger, which leads to a better detection performance with the use of a noise-reduction module.

In Fig. 11, the BER performance of CTIM-DCSK system is compared with that of MC-DCSK system. These results show that the BER performance of CTIM-DCSK system is better than that of MC-DCSK system over both AWGN and multipath Rayleigh fading channels. When  $\varepsilon = \frac{10}{\beta T_c}$ , the performance improvements of the CTIM-DCSK system are about 5 dB and 4 dB compared to the MC-DCSK system at a BER of  $10^{-5}$  over the AWGN and multipath Rayleigh fading channels, respectively. Moreover, when  $\varepsilon$  increases from  $\frac{10}{\beta T_c}$  to  $\frac{20}{\beta T_c}$ , the CTIM-DCSK system achieves gains ranging from about 5 dB to 5.5 dB compared with the MC-DCSK system at a BER of  $10^{-5}$  over the AWGN channel. Similar observations can be also drawn from the results over the multipath Rayleigh fading channel.

In Fig. 12, we compare the BER performance of CTIM-

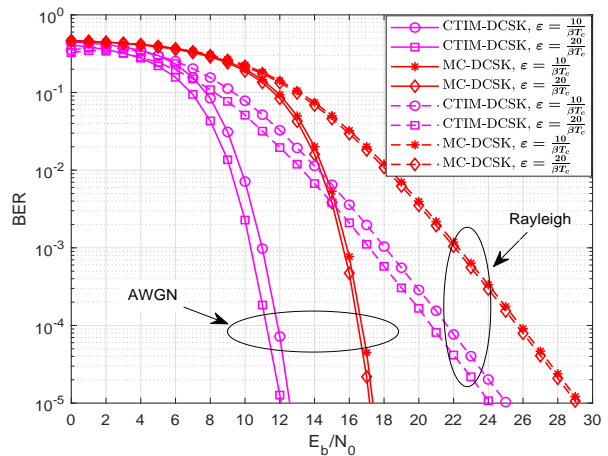


Fig. 11. BER performance of the proposed CTIM-DCSK and MC-DCSK systems over AWGN and multipath Rayleigh fading channels, where  $\beta = 450$ .

DCSK system with DCSK-DIM system over AWGN and multipath Rayleigh fading channels. In particular, the CTIM-DCSK system is superior to the DCSK-DIM system over both AWGN channel and multipath Rayleigh fading channel. For example, when  $\varepsilon = \frac{10}{\beta T_c}$ , the CTIM-DCSK system achieves a desirable BER of  $10^{-5}$  at  $E_b/N_0 = 12.6$  dB, while the DCSK-DIM system accomplishes a BER of only  $1.1 \times 10^{-2}$  over the AWGN channel. Moreover, the performance benefit of the CTIM-DCSK system further improves compared with the DCSK-DIM system as  $\varepsilon$  increases. Specifically, the CTIM-DCSK system possesses performance gains of about 3.5 dB and 4 dB with respect to the DCSK-DIM system at a BER of  $10^{-5}$  when  $\varepsilon$  equal  $\frac{10}{\beta T_c}$  and  $\frac{20}{\beta T_c}$ , respectively, over the AWGN channel.

In Figs. 10 ~ 12, the BER performance of the proposed CTIM-DCSK system is better than those of the MC-DCSK, CI-DCSK, and DCSK-DIM systems. The reason is that the proposed CTIM-DCSK system develops a new IM-DCSK signal format by intelligently incorporating frequency-and-time resources into the DCSK signals and introduces a noise-reduction design at receiver. Especially, in the new CTIM-DCSK signal, the time slots used by the selected subcarriers convey the same index bits so as to simultaneously boost the BER performance and reduce the system complexity.

Note that the CTIM-DCSK system cannot achieve the same data rate as the JTFIM-MM-DCSK [52], and MIM-DCSK [54] systems due to their different signal formats. Hence, we will select the data rates as same as possible for comparison.

Fig. 13 compares the BER results of the proposed CTIM-DCSK system with that of the JTFIM-MM-DCSK system over AWGN and multipath Rayleigh fading channels. In this figure, when  $\varepsilon = \frac{9}{\beta T_c}$  and  $\varepsilon = \frac{18}{\beta T_c}$ , the parameters of the JTFIM-MM-DCSK system are set as  $N = 2$ ,  $N_s = 1$ ,  $Q = 3$ ,  $Q_s = 2$  and  $N = 7$ ,  $N_s = 1$ ,  $Q = 2$ ,  $Q_s = 1$ , respectively. As can be seen, the BER performance of the CTIM-DCSK outperforms that of the JTFIM-MM-DCSK system. This is because that the detection of the carrier index bits of the JTFIM-MM-DCSK system affects the detection of the time index bits, which leads

<sup>1</sup>Unless otherwise specified, the above parameter setting will be adopted in the remaining simulations. Actually, it is a fair to compare BER performance between the proposed CTIM-DCSK system with its counterparts with similar data rates.

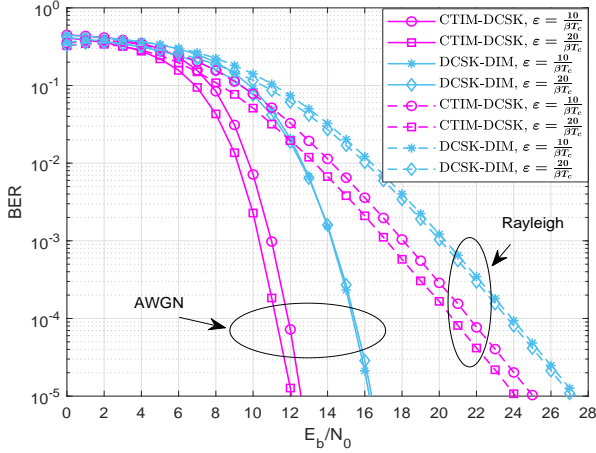


Fig. 12. BER performance of the proposed CTIM-DCSK and DCSK-DIM systems over AWGN and multipath Rayleigh fading channels, where  $\beta = 450$ .

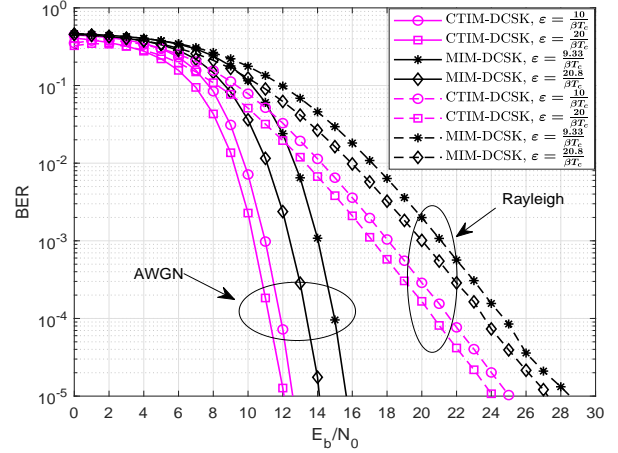


Fig. 14. BER performance of the proposed CTIM-DCSK and MIM-DCSK systems over AWGN and multipath Rayleigh fading channels, where  $\beta = 450$ .

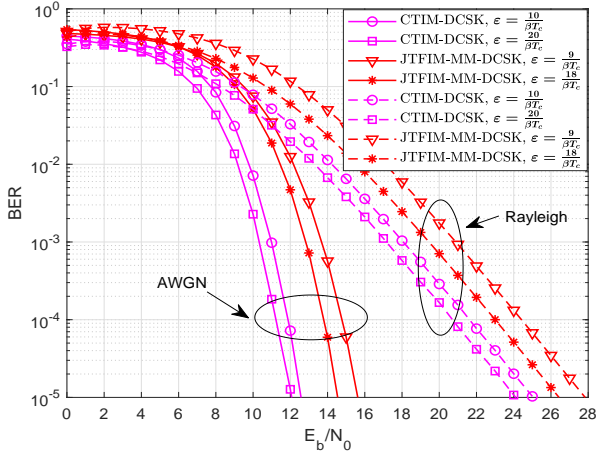


Fig. 13. BER performance of the proposed CTIM-DCSK and JTFIM-MM-DCSK systems over AWGN and multipath Rayleigh fading channels, where  $\beta = 450$ .

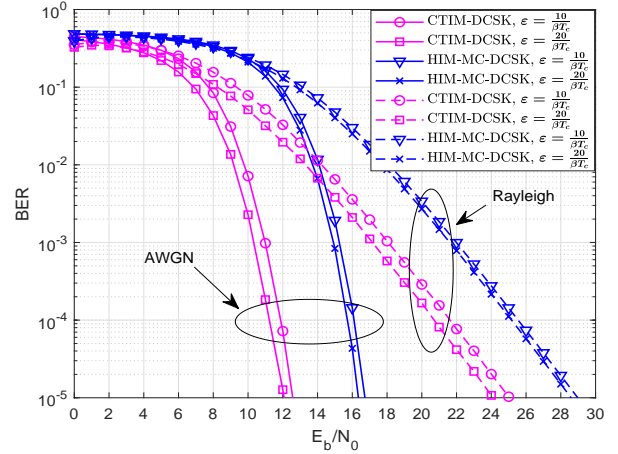


Fig. 15. BER performance of the proposed CTIM-DCSK and HIM-MC-DCSK systems over AWGN and multipath Rayleigh fading channels, where  $\beta = 450$ .

to some performance loss. For example, when  $\varepsilon = \frac{20}{\beta T_c}$ , the CTIM-DCSK system can obtain about 2.5 dB performance gain over the JTFIM-MM-DCSK system at a BER of  $10^{-5}$  over a multipath Rayleigh fading channel.

The BER performance of the CTIM-DCSK system and MIM-DCSK system is presented in Fig. 14. The main simulation parameters for MIM-DCSK system are set as  $\varepsilon = \frac{9.33}{\beta T_c}$  ( $N = 4, Q = 2, M = 4$ ), and  $\varepsilon = \frac{20.8}{\beta T_c}$  ( $N = 4, Q = 4, M = 8$ ), respectively. As can be observed, the BER performance of the CTIM-DCSK system is better than that of the MIM-DCSK system. This is due to the fact that the detection of the time index bits in the MIM-DCSK system will inevitably be affected by the wrong carrier index bits. For instance, when the data rate equals  $\varepsilon = \frac{20}{\beta T_c}$ , the CTIM-DCSK system can achieve 3 dB performance gain compared with the MIM-DCSK system at a BER of  $10^{-5}$  over a multipath Rayleigh fading channel.

Fig. 15 shows the BER performance of the CTIM-DCSK system and HIM-MC-DCSK system. The simulation param-

eters of the HIM-MC-DCSK system are set as  $\varepsilon = \frac{10}{\beta T_c}$  (i.e.,  $N = 5$ ) and  $\varepsilon = \frac{20}{\beta T_c}$  (i.e.,  $N = 10$ ), respectively. It can be seen that the CTIM-DCSK system can achieve a better BER performance in contrast to the HIM-MC-DCSK system over AWGN channel and multipath Rayleigh fading channel. For example, when  $\varepsilon = \frac{20}{\beta T_c}$ , the CTIM-DCSK system achieves a desirable BER of  $10^{-5}$  at  $E_b/N_0 = 24$  dB, while the HIM-MC-DCSK system accomplishes a BER of only  $2.157 \times 10^{-4}$  over a multipath Rayleigh fading channel.

*Remark:* We have also performed simulations for the DCSK systems with other parameter settings (e.g.,  $N, Q, \beta, \varepsilon, L, E[\lambda_l^2]$ , and  $\tau_l$ ), and have obtained similar observations.

## VI. CONCLUSION

We have designed a carrier-time-index-modulation-aided DCSK system in this paper, referred to as CTIM-DCSK system. In the proposed CTIM-DCSK system, we have provided two additional dimensions of resources for informa-

tion transmission. Through such a manner, some addition information bits can be conveyed by the carrier and time indices. Besides, the proposed CTIM-DCSK system employs a noise-reduction module at the receiver to improve the BER performance. Moreover, we have derived the analytical BER formulas of CTIM-DCSK system over AWGN as well as multipath Rayleigh fading channels, which are in good agreement with the simulation results. As a further insight, we have carefully analyzed the complexity of the proposed CTIM-DCSK system. In particular, the complexity of the CTIM-DCSK system is lower than those of the JTFIM-MM-DCSK, MIM-DCSK, HIM-MC-DCSK, MC-DCSK, DCSK-DIM, and conventional DCSK systems, but it is slightly higher than the CI-DCSK system. We have also discussed the data rate and spectral efficiency of the proposed CTIM-DCSK system. With respect to the HIM-MC-DCSK, the CI-DCSK, the MC-DCSK, and conventional DCSK systems, the proposed CTIM-DCSK system has significant improvements in terms of data rate and spectral efficiency. Owing to the above advantages, the proposed CTIM-DCSK system appears to be an outstanding candidate for Internet of Things, such as low-complexity and low-power wireless local area network (WLAN) and wireless personal area network (WPAN) applications.

#### REFERENCES

- [1] G. Kaddoum, "Wireless chaos-based communication systems: A comprehensive survey," *IEEE Access*, vol. 4, pp. 2621–2648, May 2016.
- [2] H. P. Ren, S. L. Guo, C. Bai, and X. H. Zhao, "Cross correction and chaotic shape-forming filter based quadrature multi-carrier differential chaos shift keying communication," *IEEE Trans. Veh. Technol.*, vol. 70, no. 12, pp. 12 675–12 690, Dec. 2021.
- [3] F. J. Escribano, G. Kaddoum, A. Wagemakers, and P. Giard, "Design of a new differential chaos-shift-keying system for continuous mobility," *IEEE Trans. Commun.*, vol. 64, no. 5, pp. 2066–2078, May 2016.
- [4] T. L. Carroll and L. M. Pecora, "Synchronizing chaotic circuits," *IEEE Trans. Circuits Syst.*, vol. 38, no. 4, pp. 453–456, Apr. 1991.
- [5] L. M. Pecora and T. L. Carroll, "Synchronized chaotic signals and systems," in *Proc. IEEE Int. Conf. Acoust., Speech, Signal Process.*, Aug. 1992, pp. 137–140 vol.4.
- [6] H. Dedieu, M. P. Kennedy, and M. Hasler, "Chaos shift keying: Modulation and demodulation of a chaotic carrier using self-synchronizing Chua's circuits," *IEEE Trans. Circuits Syst. II, Analog Digit. Signal Process.*, vol. 40, no. 10, pp. 634–642, Oct. 1993.
- [7] G. Kolumbán, B. Vizvári, W. Schwarz, and A. Abel, "Differential chaos shift keying: A robust coding for chaos communication," in *Proc. IEEE Workshop Nonlinear Dyn. Electron. syst., Seville, Spain.*, Jun. 1996, pp. 88–92.
- [8] Y. Fang, J. Xu, L. Wang, and G. Chen, "Performance of MIMO relay DCSK-CD systems over nakagami fading channels," *IEEE Trans. Circuits Syst. I, Reg. Papers*, vol. 60, no. 3, pp. 757–767, Mar. 2013.
- [9] C. Bai, R. Hai-Peng, and J. Li, "A differential chaos-shift keying scheme based on hybrid system for underwater acoustic communication," in *Proc. IEEE/OES China Ocean Acoust.*, Aug. 2016, pp. 1–5.
- [10] Y. Fang, G. Han, P. Chen, F. C. M. Lau, G. Chen, and L. Wang, "A survey on DCSK-based communication systems and their application to UWB scenarios," *IEEE Commun. Surv. Tutor.*, vol. 18, no. 3, pp. 1804–1837, Mar. 2016.
- [11] H. Ma, G. Cai, Y. Fang, J. Wen, P. Chen, and S. Akhtar, "A new enhanced energy-detector-based FM-DCSK UWB system for tactile Internet," *IEEE Trans. Ind. Informat.*, vol. 15, no. 5, pp. 3028–3039, May 2019.
- [12] G. Cai, Y. Fang, G. Han, J. Xu, and G. Chen, "Design and analysis of relay-selection strategies for two-way relay network-coded DCSK systems," *IEEE Trans. Veh. Technol.*, vol. 67, no. 2, pp. 1258–1271, Feb. 2018.
- [13] G. Kaddoum, H. V. Tran, L. Kong, and M. Atallah, "Design of simultaneous wireless information and power transfer scheme for short reference DCSK communication systems," *IEEE Trans. Commun.*, vol. 65, no. 1, pp. 431–443, Jan. 2017.
- [14] L. Dai, Y. Fang, Z. Yang, P. Chen, and Y. Li, "Protograph LDPC-coded BICM-ID with irregular CSK mapping in visible light communication systems," *IEEE Trans. Veh. Technol.*, vol. 70, no. 10, pp. 11 033–11 038, Oct. 2021.
- [15] Y. Fang, Y. Bu, P. Chen, F. C. M. Lau, and S. A. Otaibi, "Irregular-mapped protograph LDPC-coded Modulation: a bandwidth-efficient solution for 6G-enabled mobile networks," *IEEE Trans. Intell. Transp. Syst.*, pp. 1–14, Nov. 2021.
- [16] H. Yang and G. Jiang, "High-efficiency differential-chaos-shift-keying scheme for chaos-based noncoherent communication," *IEEE Trans. Circuits Syst. II, Exp. Briefs*, vol. 59, no. 5, pp. 312–316, May 2012.
- [17] W. Xu, L. Wang, and G. Kolumbán, "A novel differential chaos shift keying modulation scheme," *Int. J. Bifurcat. Chaos*, vol. 21, no. 3, pp. 799–814, Mar. 2011.
- [18] —, "A new data rate adaption communications scheme for code-shifted differential chaos shift keying modulation," *Int. J. Bifurcat. Chaos*, vol. 22, no. 8, pp. 1–8, Aug. 2012.
- [19] G. Kaddoum, E. Soujeri, C. Arcila, and K. Eshteiwi, "I-DCSK: An improved noncoherent communication system architecture," *IEEE Trans. Circuits Syst. II, Exp. Briefs*, vol. 62, no. 9, pp. 901–905, Sept. 2015.
- [20] H. Yang, W. K. S. Tang, G. Chen, and G. P. Jiang, "System design and performance analysis of orthogonal multi-level differential chaos shift keying modulation scheme," *IEEE Trans. Circuits Syst. I, Reg. Papers*, vol. 63, no. 1, pp. 146–156, Jan. 2016.
- [21] G. Cai, Y. Fang, and G. Han, "Design of an adaptive multire solution  $M$ -ary DCSK system," *IEEE Commun. Lett.*, vol. 21, no. 1, pp. 60–63, Jan. 2017.
- [22] Y. Tan, W. Xu, and S. Hong, "An  $M$ -ary code shifted differential chaos shift keying scheme," in *Proc. IEEE Asia-Pac. Conf. Commun.*, 2017, pp. 1–6.
- [23] X. Cai, W. Xu, and S. Hong and L. Wang, "A trinal-code shifted differential chaos shift keying system," *IEEE Commun. Lett.*, vol. 25, no. 3, pp. 1000–1004, Mar. 2021.
- [24] G. Kaddoum, F. Richardson, and F. Gagnon, "Design and analysis of a multi-carrier differential chaos shift keying communication system," *IEEE Trans. Commun.*, vol. 61, no. 8, pp. 3281–3291, Aug. 2013.
- [25] M. Wen, Q. Li, E. Basar, and W. Zhang, "Generalized multiple-mode OFDM with index modulation," *IEEE Trans. Wireless Commun.*, vol. 17, no. 10, pp. 6531–6543, Oct. 2018.
- [26] E. Basar, "Index modulation techniques for 5G wireless networks," *IEEE Commun. Mag.*, vol. 54, no. 7, pp. 168–175, Jul. 2016.
- [27] H. Ma, Y. Fang, G. Cai, G. Han, and Y. Li, "A new frequency-bin-index LoRa system for high-data-rate transmission: Design and performance analysis," *IEEE Internet Things J.*, vol. 9, no. 14, pp. 12515–12528, Jul. 2022.
- [28] H. Ma, G. Cai, Y. Fang, P. Chen, and G. Chen, "Design of a superposition coding PPM-DCSK system for downlink multi-user transmission," *IEEE Trans. Veh. Technol.*, vol. 69, no. 2, pp. 1666–1678, Feb. 2020.
- [29] R. Y. Mesleh, H. Haas, S. Sinanovic, C. W. Ahn, and S. Yun, "Spatial modulation," *IEEE Trans. Veh. Technol.*, vol. 57, no. 4, pp. 2228–2241, Jul. 2008.
- [30] E. Soujeri, G. Kaddoum, M. Au, and M. Herceg, "Frequency index modulation for low complexity low energy communication networks," *IEEE Access*, vol. 5, pp. 23 276–23 287, Jun. 2017.
- [31] X. Cheng, M. Zhang, M. Wen, and L. Yang, "Index modulation for 5G: striving to do more with less," *IEEE Wireless Commun.*, vol. 25, no. 2, pp. 126–132, Apr. 2018.
- [32] E. Baar and E. Panayrc, "Optical OFDM with index modulation for visible light communications," in *Proc. IEEE Int. Workshop Opt. Wireless Commun.*, Sept. 2015, pp. 11–15.
- [33] E. Basar, U. Aygolu, E. Panayrc, and H. V. Poor, "Orthogonal frequency division multiplexing with index modulation," *IEEE Trans. Signal Process.*, vol. 61, no. 22, pp. 5536–5549, Nov. 2013.
- [34] M. C. Gursoy, E. Basar, A. E. Pusane, and T. Tugcu, "Index modulation for molecular communication via diffusion systems," *IEEE Trans. Commun.*, vol. 67, no. 5, pp. 3337–3350, May 2019.
- [35] A. A. Purwita, A. Yesilkaya, M. Safari, and H. Haas, "Generalized time slot index modulation for optical wireless communications," *IEEE Trans. Commun.*, vol. 68, no. 6, pp. 3706–3719, Jun. 2020.
- [36] X. Yao, P. Yang, J. Fu, Y. Xiao, and Z. Liu, "A hybrid multi-domain index modulation for covert communication," *IEEE Wireless Commun. Lett.*, pp. 1–1, Sept. 2021.
- [37] G. Cai, Y. Fang, P. Chen, G. Han, G. Cai, and Y. Song, "Design of an MISO-SWIPT-aided code-Index modulated multi-carrier  $M$ -DCSK system for e-health IoT," *IEEE J. Sel. Areas Commun.*, vol. 39, no. 2, pp. 311–324, Feb. 2021.

- [38] X. Cai, W. Xu, F. C. M. Lau, and L. Wang, "Joint carrier-code index modulation aided  $M$ -ary differential chaos shift keying system," *IEEE Trans. Veh. Technol.*, vol. 69, no. 12, pp. 15 486–15 499, Dec. 2020.
- [39] X. Cai, W. Xu, S. Hong, L. Wang, and L. Zhang, "General carrier index aided dual-mode differential chaos shift keying with full mapping: Design and optimization," *IEEE Trans. Veh. Technol.*, vol. 70, no. 11, pp. 11 665–11 677, Nov. 2021.
- [40] Z. Liu, L. Zhang, Z. Wu, and Y. Jiang, "Energy efficient parallel concatenated index modulation and  $M$ -ary PSK aided OFDM-DCSK communications with QoS consideration," *IEEE Trans. Veh. Technol.*, vol. 69, no. 9, pp. 9469–9482, Sept. 2020.
- [41] H. Zhang, L. Zhang, Y. Jiang, and Z. Wu, "Reliable and secure deep learning-based OFDM-DCSK transceiver design without delivery of reference chaotic sequences," *IEEE Trans. Veh. Technol.*, vol. 71, no. 8, pp. 8059–8074, Aug. 2022.
- [42] W. Xu, Y. Tan, F. C. M. Lau, and G. Kolumbán, "Design and optimization of differential chaos shift keying scheme with code index modulation," *IEEE Trans. Commun.*, vol. 66, no. 5, pp. 1970–1980, May 2018.
- [43] W. Xu, T. Huang, and L. Wang, "Code-shifted differential chaos shift keying with code index modulation for high data rate transmission," *IEEE Trans. Commun.*, vol. 65, no. 10, pp. 4285–4294, Oct. 2017.
- [44] X. Cai, W. Xu, M. Miao, and L. Wang, "Design and performance analysis of a new  $M$ -ary differential chaos shift keying with index modulation," *IEEE Trans. Wireless Commun.*, vol. 19, no. 2, pp. 846–858, Feb. 2020.
- [45] G. Cheng, L. Wang, W. Xu, and G. Chen, "Carrier index differential chaos shift keying modulation," *IEEE Trans. Circuits Syst. II, Exp. Briefs*, vol. 64, no. 8, pp. 907–911, Aug. 2017.
- [46] G. Cheng, X. Chen, W. Liu, and W. Xiao, "GCI-DCSK: Generalized carrier index differential chaos shift keying modulation," *IEEE Commun. Lett.*, vol. 23, no. 11, pp. 2012–2016, Nov. 2019.
- [47] X. Cai, W. Xu, L. Wang, and F. Xu, "Design and performance analysis of differential chaos shift keying system with dual-index modulation," *IEEE Access*, vol. 7, pp. 26 867–26 880, Feb. 2019.
- [48] S. Doğan Tusha, A. Tusha, E. Basar, H. Arslan, "Multidimensional index modulation for 5G and beyond wireless networks," *Proc. IEEE*, vol. 109, no. 2, pp. 190–199, Feb. 2021.
- [49] X. Wang, Q. Zhang, R. Gao, X. Wang, X. Xin, F. Tian, Q. Tian, Y. Wang, D. Guo, and H. Chang, "Multidimensional modulation method based on grouped subcarrier index modulated OFDM," in *Proc. IEEE Int. Conf. Opt. Commun. Networks*, pp. 1–3, Oct. 2021.
- [50] S. Lu, I. A. Hemadeh, M. El-Hajjar, and L. Hanzo, "Compressed sensing-aided multi-dimensional index modulation," *IEEE Trans. Commun.*, vol. 67, no. 6, pp. 4074–4087, Jun. 2019.
- [51] B. Shamasundar, S. Bhat, S. Jacob, and A. Chockalingam, "Multidimensional index modulation in wireless communications," *IEEE Access*, vol. 6, pp. 589–604, Nov. 2018.
- [52] X. Cai, W. Xu, L. Wang, and G. Chen, "Towards high-data-rate noncoherent chaotic communication: A multiple-mode differential chaos shift keying system," *IEEE Trans. Wireless Commun.*, vol. 20, no. 8, pp. 4888–4901, Aug. 2021.
- [53] Y. Tao, Y. Fang, H. Ma, S. Mumtaz, and M. Guizani, "Multi-carrier DCSK with hybrid index modulation: A new perspective on frequency-index-aided chaotic communication," *IEEE Trans. Commun.*, vol. 70, no. 6, pp. 3760–3773, Apr. 2022.
- [54] H. Ma, Y. Fang, P. Chen, S. Mumtaz, and Y. Li, "A novel differential chaos keying scheme with multidimensional index modulation," *IEEE Trans. Wireless Commun.*, vol. 22, no. 1, pp. 237–256, Jan. 2023.
- [55] T. Michail, B. Christina, and H. Hossein, "On the folded normal distribution," *Mathematics*, vol. 2, no. 1, pp. 12–28, Feb. 2014.
- [56] H. Ma, G. Cai, Y. Fang, P. Chen, and G. Han, "Design and performance analysis of a new STBC-MIMO LoRa system," *IEEE Trans. Commun.*, vol. 69, no. 9, pp. 5744–5757, Sept. 2021.
- [57] H. Ma, Y. Fang, P. Chen, and Y. Li, "Reconfigurable intelligent surface-aided  $M$ -ary FM-DCSK system: A new design for noncoherent chaos-based communication," *IEEE Trans. Veh. Technol.*, pp. 1–15, Dec. 2022.
- [58] M. W. Wen, X. Y. Cheng, and L. Q. Yang, *Index modulation for 5G wireless communications*. Springer, Dec. 2017.



**Yi Fang** (Senior Member, IEEE) received the Ph.D. degree in communication engineering, Xiamen University, China, in 2013. From May 2012 to July 2012, He was a Research Assistant in electronic and information engineering, Hong Kong Polytechnic University, Hong Kong. From September 2012 to September 2013, he was a Visiting Scholar in electronic and electrical engineering, University College London, UK. From February 2014 to February 2015, he was a Research Fellow at the School of Electrical and Electronic Engineering, Nanyang Technological University, Singapore. He is currently a Full Professor and Vice Dean at the School of Information Engineering, Guangdong University of Technology, China. He served as the Publicity Co-Chair of the International Symposium on Turbo Codes and Iterative Information Processing 2018. His current research interests include information and coding theory, spread-spectrum modulation, and cooperative communications.



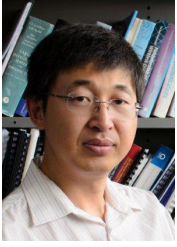
**Junming Zhuo** received the B.Sc. degree in optoelectronic information science and engineering from South China Agricultural University, Guangzhou, China, in 2020. He is currently pursuing the M.Sc. degree with the Department of Communication Engineering, Guangdong University of Technology, Guangzhou, China. His primary research interests include spread-spectrum modulation and the Internet of Things.



**Huan Ma** (Graduate Student Member, IEEE) received the B.Sc. degree in communication engineering from Heilongjiang University, Harbin, China, in 2017, and the M.Sc. degree in electronic and communication engineering from Guangdong University of Technology, Guangzhou, China, in 2020. He is currently pursuing the Ph.D. degree with the Department of Communication Engineering, Guangdong University of Technology, Guangzhou, China. His primary research interests include spread-spectrum modulation and Internet of Things.



**Shahid Mumtaz** (Senior Member, IEEE) is an IET Fellow, IEEE ComSoc and ACM Distinguished speaker, recipient of IEEE ComSoc Young Researcher Award (2020), founder and EIC of I-ET "Journal of Quantum communication," Vice-Chair: Europe/Africa Region- IEEE ComSoc: Green Communications & Computing society and Vice-chair for IEEE standard on P1932.1: Standard for Licensed/Unlicensed Spectrum Interoperability in Wireless Mobile Networks. He is the author of 4 technical books, 12 book chapters, 300+ technical papers (200+ IEEE Journals/transactions, 100+ conference, 2 IEEE best paper award- in the area of mobile communications. Most of his publication is in the field of Wireless Communication. He is serving as Scientific Expert and Evaluator for various Research Funding Agencies. He was awarded an "Alain Bensoussan fellowship" in 2012. He is the recipient of the NSFC Researcher Fund for Young Scientist in 2017 from China.



**Yonghui Li** (Fellow, IEEE) received his PhD degree in November 2002 from Beijing University of Aeronautics and Astronautics. Since 2003, he has been with the Centre of Excellence in Telecommunications, the University of Sydney, Australia. He is now a Professor and Director of Wireless Engineering Laboratory in School of Electrical and Information Engineering, University of Sydney. He is the recipient of the Australian Queen Elizabeth II Fellowship in 2008 and the Australian Future Fellowship in 2012. He is a Fellow of IEEE. His

current research interests are in the area of wireless communications, with a particular focus on MIMO, millimeter wave communications, machine to machine communications, coding techniques and cooperative communications. He holds a number of patents granted and pending in these fields. He is now an editor for IEEE transactions on communications, IEEE transactions on vehicular technology. He also served as the guest editor for several IEEE journals, such as IEEE JSAC, IEEE Communications Magazine, IEEE IoT journal, IEEE Access. He received the best paper awards from IEEE International Conference on Communications (ICC) 2014, IEEE PIRMC 2017 and IEEE Wireless Days Conferences (WD) 2014.